Journal of Materials Chemistry A

Accepted Manuscript

ROYAL SOCIETY OF CHEMISTRY

www.rsc.org/materialsA

Journal Name

ARTICLE

Manganese oxides supported on hydrogenated TiO_2 nanowire arrays catalysts for electrochemical oxygen evolution reaction in water electrolysis

Received 00th January 20xx,
Accepted 00th January 20xx

DOI: 10.1039/x0xx00000x

www.rsc.org/

Nan Li,[a] Wei-Yan Xia,[a] Jing Wang,[a] Zi-Li Liu,[a] Qing-Yu Li,[b] Sheng-Zhou Chen,[a] Chang-Wei Xu,[a]* and Xi-Hong Lu,[c]*

Hydrogenated TiO_2/MnO_x nanowires (NWs) with a diameter of 50~80 nm and a length of 0.5~0.8 μm supported on carbon cloth have been successfully prepared. The entire surface of the H-TiO_2 NWs is covered uniformly by amorphous MnO_x with an average thickness of 7.0 nm. The H-TiO_2 NWs are poorly active for oxygen evolution reaction (OER) and the MnO_x as a major potential feasible electrocatalyst shows a considerable activity. The onset potential shifts negatively and current density improves not only by the enlarged surface area of MnO_x support on the H-TiO_2 NWs, but also by a synergistic effect between TiO_2 and MnO_x. The presence of three valence manganese oxides such as MnO, Mn_2O_3 and MnO_2 in the H-TiO_2/MnO_x NWs is apt to occur the OER due to electron transfer. The percentage of Mn^{2+} increases and the percentage of Mn^{3+} and Mn^{4+} decreases after test, which prove the assume that the Mn^{4+} is firstly reduced to Mn^{3+} by electron injection from H_2O, then Mn^{3+} is further reduced to Mn^{2+} when the O_2 evolution happens for the OER in the alkaline media at pH ≥ 9.

Introduction

The demand for renewable energy sources which are environmentally friendly is growing to take the place of fossil fuels due to continuous consumption of fossil fuels and ever-increasing environmental problems. Wind and solar energy systems are the most well-known renewable energy sources which are used as power generation systems.[1] However, the power output of wind and solar energy systems is dependent on climatic and geographic conditions.[2] One promising alternative is hydrogen, which has the great advantage that it can be produced by coupling renewable energies such as wind and solar energies with water electrolysis.[3–6] Hydrogen is a suitable option and it can be used as a fuel to get a reliable power for almost every application that fossil fuels are used. Furthermore, hydrogen can be converted in other types of energies more efficiently than fossil fuels.[2] By the way, hydrogen produced with water electrolysis is without carbon monoxide which will poise the Pt catalyst in the proton exchange membrane fuel cell.

Electrochemical hydrogen evolution from water splitting has attracted more and more attention in alkaline media. In alkaline media, electrochemical water electrolysis consists of two half-reactions: the cathodic hydrogen evolution reaction (HER, $2H_2O + 2e = 2OH^- + H_2$) and the anodic oxygen evolution reaction (OER, $4OH^- = 2H_2O + 4e + O_2$). Of two half-reactions, the OER requires formation of two oxygen-oxygen bonds in the four-electron redox processes, which results in more kinetically demanding for the OER.[7–9] So, the OER needs relatively high overpotential at the anode. The high overpotential in the irreversible OER is a major cause of high energy consumption. Thus, a lot of efforts have been devoted to explore the electrocatalysts with low OER overpotential. The rutiletype oxides of RuO_2 and IrO_2 show the lowest OER overpotential, however theses oxides suffer from poor chemical stability in alkaline media and the high price and limited supply of Ru and Ir.[10–17] So other metal oxides such as Co oxide, Ni oxide, $NiCo_2O_4$, Ni-Li oxide, Ni-Fe oxide and Zn-Co oxide have been developed.[18–33] Manganese is earth-abundant element and the manganese oxides have been already demonstrated to have high activity for the OER.[34–41] For further enhancement the OER properties, considerable efforts have been devoted to explore the electrocatalysts with low OER overpotential by adding second element. As we known, the catalyst activity of manganese oxides for the OER will be enhanced by Pt, Pd and Au.[42–45] However, the high price and limited supply of Pt, Pd and Au are major barriers to the development of OER using Pt-based, Pd-based catalysts and Au-based catalysts. Therefore, researchers are making their efforts to study high-performance catalysts without noble-metals. For instance, Gao and his cooperators reported that $Mn_3O_4/CoSe_2$ displays a superior OER performance relative to parent $CoSe_2$ nanobelts.[46] Titanium oxide modified catalysts, especially IrO_2-TiO_2, have been particularly recognized as the most efficient electrocatalysts for the OER.[47,48] Cai and his cooperators presented a controllable and reliable sol-flame doping method for the synthesis of TiO_2:Co nanowires (NWs) that exhibit significantly enhanced electrocatalytic activity for the OER.[49]

[a] Guangzhou Key Laboratory for Environmentally Functional Materials and Technology, School of Chemistry and Chemical Engineering, Guangzhou University, Guangzhou 510006, China. E-mail: cwxu@gzhu.edu.cn
[b] Guangxi Key Laboratory of Low Carbon Energy Materials, School of Chemistry and Pharmaceutical Sciences, Guangxi Normal University, Guilin 541004, China
[c] MOE of the Key Laboratory of Bioinorganic and Synthetic Chemistry, School of Chemistry and Chemical Engineering, Sun Yat-Sen University, Guangzhou 510275, China. E-mail: luxh6@mail.sysu.edu.cn
† Footnotes relating to the title and/or authors should appear here.

In this paper, one dimensional (1D) core-shell TiO_2/MnO_x NWs arrays were grown directly on carbon cloth substrate which is flexible conductive substrate. Hydrogen-treated TiO_2 (denoted as H-TiO_2) NWs as the core (conducting scaffold) to support electrochemically active MnO_x. In comparison to bulk materials, the 1D NWs arrays such as nanowire/nanorod arrays are the most attractive materials due to their high interfacial area between electrode and electrolyte for charge transport and fast electrical pathways among the numerous nanostructures.[49–55] Depend on the recent research, such structure permits reactants to diffuse into the catalyst layer easily and form a larger three-phase interface, resulting in the reduction of liquid sealing effect, hence improve the catalyst performance.[56] Lei and his cooperators have reported that Ni–Co–O@Ni–Co–S hierarchical NWs arrays show a significantly improved activity for the OER.[57] Wang and his cooperators have reported that hierarchically Ni_3S_2 nanorod arrays exhibit with low overpotential of 200 and 217 mV at current density of 10 mA cm^2 for HER and OER, which are the best non-noble metal HER/OER electrocatalysts reported in literatures.[58]The hierarchical NWs arrays can offer a higher surface area and porosity, while the conductivity can be well preserved. The hierarchical porosity could accelerate the diffusion of the OH^- ions, thus resulting in faster kinetics.

Experimental

TiO_2 NWs were grown on the carbon cloth substrate by a seed-assisted hydrothermal method reported elsewhere.[56] Carbon cloth (6.0 cm x 3.0 cm) was cleaned with ethanol and distilled water and then dried at room temperature. The pre-cleaned carbon cloth was immersed into 0.2 mol L^{-1} titanium (IV) chloride aqueous solution for 10 min and blow-dried with compressed air. And then the carbon cloth was heated on a hotplate in air at 350°C for 10 min to form TiO_2 nanoparticles on the carbon cloth surface (TiO_2 nanoparticle seeded substrate). Hydrochloric acid (37%) with 15 mL was diluted with 15 mL deionized water, and mixed with 0.45 mL titanium n-butoxide. This solution mixture and the seeded carbon cloth were transferred to a Teflon-lined stainless steel autoclave (40 mL volume). The sealed autoclave was heated in an electric oven at 150°C for 5 h, and then it cooled down slowly at room temperature. A TiO_2 NWs film was uniformly coated on the carbon cloth surface. The sample was thoroughly washed with deionized water and then air dried, and then annealed in air at 550°C for 1 h and then hydrogenated at 800°C for an additional hour to form H-TiO_2 NWs. H-TiO_2/MnO_x NWs were obtained by depositing a MnO_x thin layer onto the surface of H-TiO_2 NWs by anodic electrodeposition. The electrodeposition was conducted in a solution (15 mL) containing manganese acetate (0.1 mol L^{-1}) and sodium sulfate (0.1 mol L^{-1}) at 1.0 V for 60 s at room temperature. MnO_x was deposited on carbon cloth under the same conditions for comparison.

X-ray diffraction (XRD) measurement was conducted on a PANalytical, PW3040/60 diffractometer with monochromatized Cu Ka radiation (λ = 0.15418 nm). The structural properties of electrode materials were characterized by field-emission scanning electron microscopy (FE-SEM, JSM-6330F), transmission electron microscopy (TEM, JEM2010-HR, 200 KV), X-ray photoelectron spectroscopy (XPS, ESCALab250, Thermo VG). All electrochemical measurements were tested in a three-electrode cell using the EG&GPAR283 electrochemical work station (Princeton, USA) in a temperature-controlled water-bath (Poly-science 9106, U.S.A.) at 298 K. Solutions were freshly prepared before each experiment. A platinum foil (3.0 cm^2) was used as counter electrode. All the potentials were measured versus a saturated calomel electrode (SCE, 0.241 V versus NHE) electrode. A salt bridge was used between the cell and the reference electrode.

Results and discussion

Chemical bonding states in the H-TiO_2/MnO_x NWs support on the carbon cloth were analyzed by XPS as shown in Figure 1. A survey of H-TiO_2/MnO_x NWs is shown in Figure 1a and the peaks are corresponding to existence of C 1s, Ti 2p, Mn 2p and O 1s. The binding energy of C 1s peak locates at 284.4 eV which is related to the graphitic carbon in the carbon cloth as shown in Figure 1a. The values of binding energy for Ti $2p_{3/2}$ and $2p_{1/2}$ typical peaks of TiO_2 (Figure 1b) are centered at 458.4 eV and 464.3 eV and these values are consistent with those in the literature.[59] The XPS spectra of Mn 2p binding energy for the H-TiO_2/MnO_x NWs are shown in Figure 1c. By performing a peak fitting deconvolution, the Mn $2p_{3/2}$ spectrum appears as three peaks: 640.8 (MnO), 642.0 (Mn_2O_3) and 643.5 (MnO_2) eV, respectively.[60–62] The value of binding energy for Mn $2p_{1/2}$ typical peak is centered at 653.8 eV. The presence of multiple valence manganese oxides in the H-TiO_2/MnO_x NWs is apt to occur redox reaction due to electron transfer. The O_{1s} spectrum can be found two components as shown in Figure 1d, suggesting the presence of two types of oxygen-containing species. The bands at 529.6 eV and 531.4 eV can be assigned to the oxygen bonds of Mn-O-Mn and Mn-OH, respectively.[63]

XRD patterns for the MnO_x, H-TiO_2 NWs, H-TiO_2/MnO_x NWs grown on the carbon cloth substrate are shown in Figure 2a. The diffraction peak at around 26.5° observed in all the samples is assigned to the (002) plane of the carbon for carbon cloth. The diffraction peaks of manganese oxides can not be found in MnO_x,

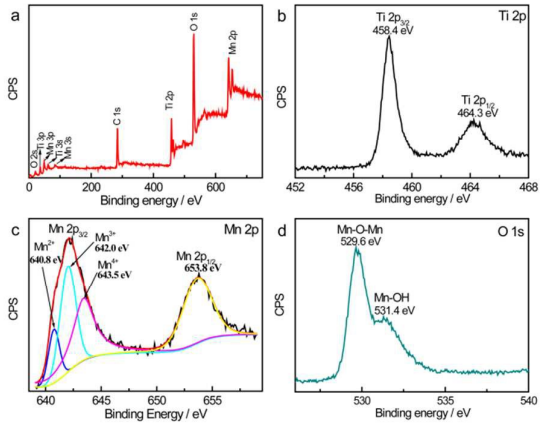

Figure 1. XPS of (a) survey, (b) Ti 2p, (c) Mn 2p, and (d) O 1s for H-TiO_2/MnO_x NWs.

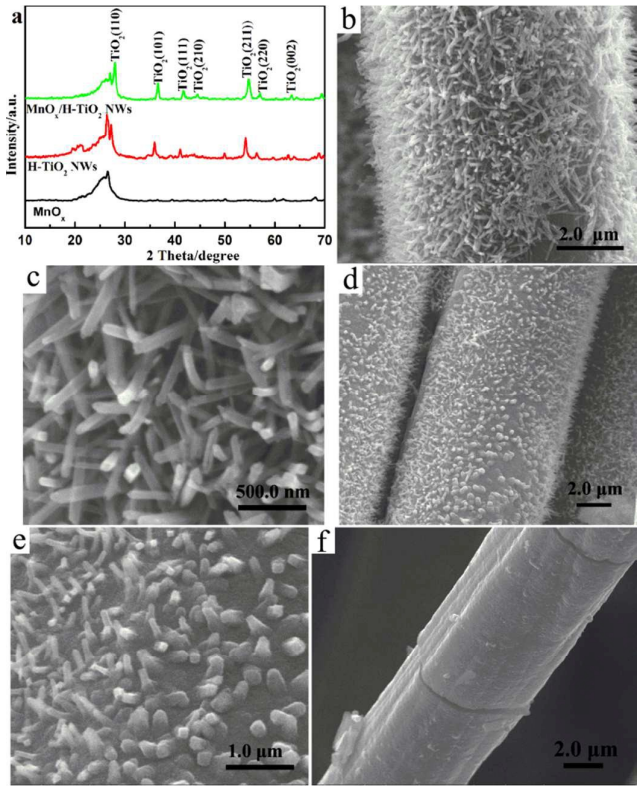

Figure 2. (a) XRD patterns for MnO_x, H-TiO_2 NWs, H-TiO_2/MnO_x NWs; (b,c) SEM images for H-TiO_2 NWs, (d,e) SEM images for H-TiO_2/MnO_x NWs, and (f) SEM image for MnO_x.

which proves that it is an amorphous material. The diffraction peaks around 27.4, 36.1, 39.2, 41.2, 54.3, 56.6, 62.8 and 64.0° are assigned to the (110), (101), (200), (111), (210), (211), (220) and (002) facets of the rutile crystallite TiO_2. In the XRD pattern of H-TiO_2/MnO_x NWs, all the diffraction peaks of TiO_2 can be found and that of manganese oxides can not be found, which also proves that MnO_x in the H-TiO_2/MnO_x NWs is an amorphous material. Figs. 2b and 2c are the SEM images of H-TiO_2 NWs on the carbon cloth and show that the entire surface of the carbon fiber on the carbon cloth is covered uniformly by H-TiO_2 NWs with a diameter of 40~70 nm and a length of 0.7~1 μm. H-TiO_2 NWs are highly ordered with uniform diameter and length. After deposited a MnO_x thin layer onto the surface of H-TiO_2 NWs by anodic electrodeposition, the NWs still exist as shown in Figs. 2d and 2e. Figure 2f is the SEM image of MnO_x on the carbon cloth and shows that the entire surface of the carbon fiber is covered by MnO_x layer with a smooth surface.

The typical TEM images of H-TiO_2/MnO_x NWs are shown in Figure 3. Figure 3a shows that the diameter is 50~80 nm and the length is 0.5~0.8 μm for the H-TiO_2/MnO_x NWs. The entire surface of the H-TiO_2 NWs is covered uniformly by MnO_x. The MnO_x shell has an average thickness of 7.0 nm as shown in high-resolution TEM (HRTEM) image (Figure 3b). In the inset figure in Figure 3b, the parallel fringe with a spacing of 0.32 nm is corresponding to the (110) plane of rutile TiO_2. From the HRTEM observation, the TiO_2 has a high crystalline nature. However, there is not parallel fringe for MnO_x. Selected-area electron diffraction (SAED) analysis confirms that H-TiO_2 growing alone the [001] axis is a single crystal. However, there is not electron diffraction for MnO_x, which also proves that MnO_x in the H-TiO_2/MnO_x NWs is an amorphous material.

In order to illustrate the advantages of the TiO_2/MnO_x NWs electrocatalyst, the OER activity of MnO_x, H-TiO_2 NWs and H-TiO_2/MnO_x NWs is evaluated through linear sweep voltammetric (LSV) curves in 0.1 mol L^{-1} KOH with a sweep rate of 0.001 V s^{-1} as shown in Figure 4. All the area of the electrodes has been controlled in 1.0 cm × 1.0 cm. The onset potential (E_s) of OER is 0.534 V on the MnO_x electrode, 0.575 V on the H-TiO_2 NWs electrode, and 0.524 V on the H-TiO_2/MnO_x NWs electrode. The lower the value of E_s is, the easier the OER happens. OER has the lowest value of E_s on the H-TiO_2/MnO_x NWs electrode, so OER happens the most easily on the H-TiO_2/MnO_x NWs electrode. The values of current density at 0.7 V ($j_{0.7V}$) are 7.4, 4.5 and 17.2 mA cm^{-2} on the MnO_x, H-TiO_2 NWs and H-TiO_2/MnO_x NWs electrodes. The value of $j_{0.7V}$ on the H-TiO_2/MnO_x NWs electrode is 2.3 and 3.8 times as bigger as that

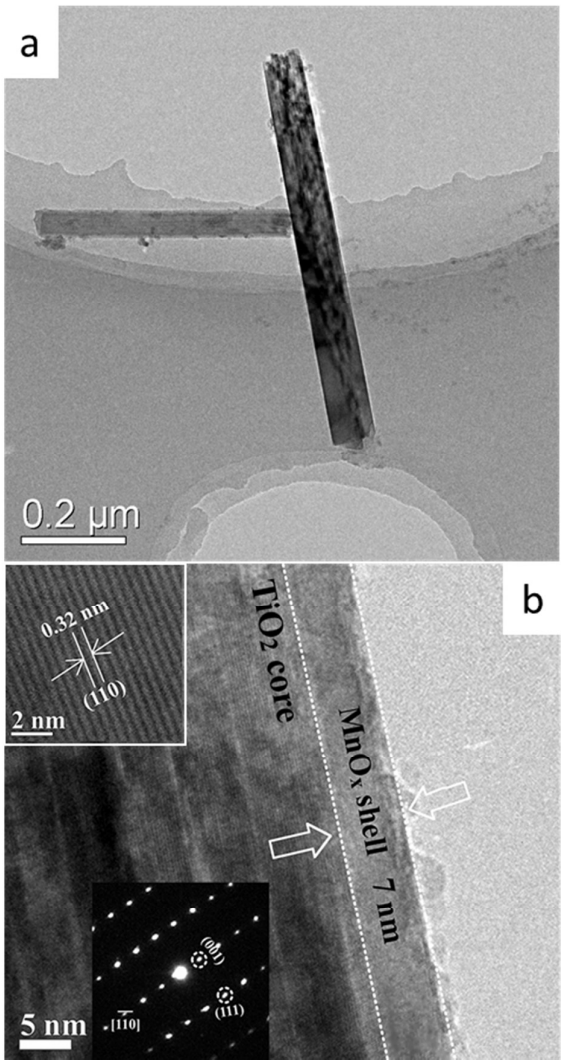

Figure 3. TEM images of H-TiO_2/MnO_x NWs. Magnified TEM image and SAED pattern in the inset figure of Figure 3b.

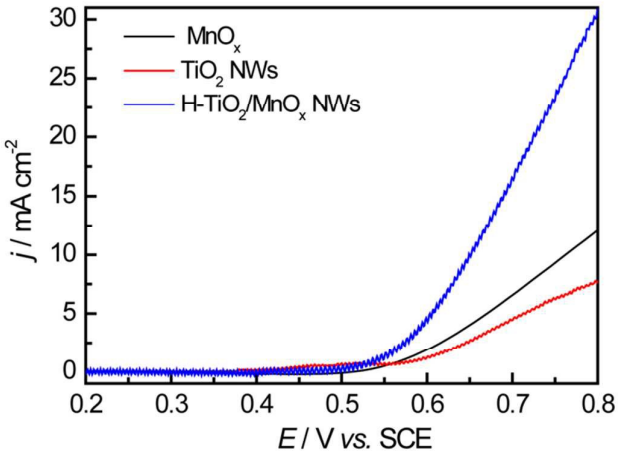

Figure 4. LSV curves in 0.1 mol L^{-1} KOH at a sweep rate of 0.001 V s^{-1}.

on the MnO_x and H-TiO_2 NWs electrodes. The H-TiO_2 NWs are poorly active for OER and the MnO_x as a major potential feasible electrocatalyst shows a considerable activity. The current density improves not only by the surface area of MnO_x support on the H-TiO_2 NWs, but also by a synergistic effect between TiO_2 and MnO_x because the value of E_s is lower and the current density is higher on the H-TiO_2/MnO_x electrode than that on the MnO_x and H-TiO_2 NWs electrode.[64,65]

The stability of OER on the all electrodes is investigated by chronoamperometry and chronopotentiometry. According to the report of Jaramillo and his cooperators, the stability loss of OER could be owing to lots of factors, such as corrosion, material degradation, surface passivation and so on.[66] Meng and his cooperators have synthesized manganese oxides of various structures (amorphous, α-, β-, and δ-MnO_2), which have been studied systematically as OER catalysts. They have observed significant material loss under long-term electrolysis.[67] The chronoamperometric curves for OER in 0.1 mol L^{-1} KOH solution under a potential of 0.7 V was shown in Figure 5a. Until the end of the experiment, the oxidation current density on the H-TiO_2/MnO_x NWs electrode is 9.8 mA cm^{-2}, which is 1.3 times as bigger as that on the MnO_x electrode (7.4 mA cm^{-2}). The result shows that OER on the H-TiO_2/MnO_x NWs electrode has a higher current density than that on the MnO_x electrode with the same potential. The chronopotentiometric curves for the OER in 0.1 mol L^{-1} KOH solution under a current density of 10 mA cm^{-2} was shown in Figure 5b. The potential requires to achieve a current density of 10 mA cm^{-2} which is an important performance index of an OER catalyst because it is approximately the current density for a 10% efficient solar-to-fuel conversion device.[66,68] In the initial several minutes, the voltages have a sharp increase. At the 20 min, the corresponding potentials are 1.20 V for the MnO_x, 1.34 V for the H-TiO_2 NWs and 1.13 V for the H-TiO_2/MnO_x NWs, then the potentials remain almost the same after the test time. The results show that OER on the H-TiO_2/MnO_x NWs electrode has a lower electrolysis potential than that on the MnO_x electrode with the same current density.

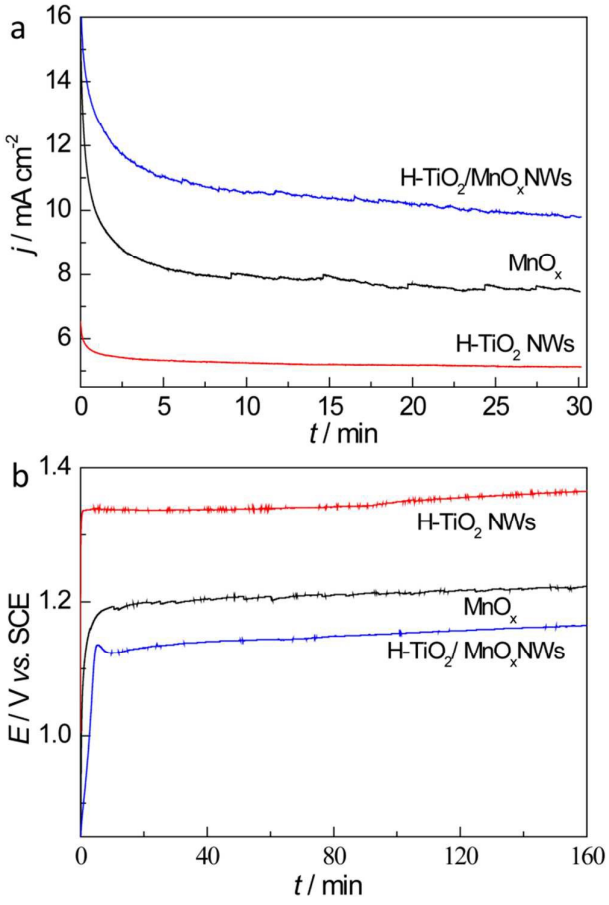

Figure 5. (a) Chronoamperometric curves under a potential of 0.7 V; and (b) chronopotentiometric curves under a current density of 10 mA cm^{-2} in 0.1 mol L^{-1} KOH solution.

The percentage of different valence for manganese oxide in the H-TiO_2/MnO_x NWs after 30 min chronoamperometry test at 0.7 V in 0.1 mol L^{-1} KOH solution was analyzed by XPS as shown in Figure 6. Before test, the percentage is 13.9% for Mn^{2+}, 39.5% for Mn^{3+} and 46.6% for Mn^{4+} in the H-TiO_2/MnO_x NWs. After test, the percentage is 23.0% for Mn^{2+}, 36.8% for Mn^{3+} and 40.6% for Mn^{4+} in the H-TiO_2/MnO_x NWs. The percentage of Mn^{2+} increases and the percentage of Mn^{3+} and Mn^{4+} decreases in the H-TiO_2/MnO_x NWs after test. Takashima and his cooperators have assumed that the Mn^{4+} is firstly reduced to Mn^{3+} by electron injection from H_2O, then Mn^{3+} is further reduced to Mn^{2+} when the O_2 evolution happens for the OER in the alkaline media at pH ≥ 9.[69] So the amount of Mn^{2+} increases and the amount of Mn^{3+} and Mn^{4+} decreases after test, which also prove the assume. Transformation between manganese oxides indicates electronic movement, and the presence of multiple valence manganese oxides on the surface of the H-TiO_2/MnO_x NWs is conducive to electron transfer.

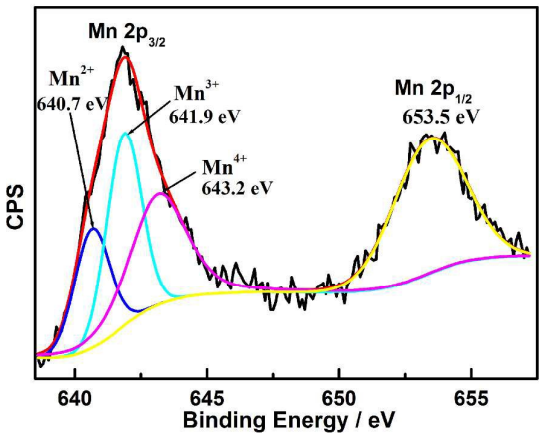

Figure 6. XPS image of Mn 2p for H-TiO_2/MnO_x NWs after 30 min chronoamperometry test at 0.7 V in 0.1 mol L^{-1} KOH solution.

Conclusions

H-TiO_2/MnO_x NWs with a diameter of 50~80 nm and a length of 0.5~0.8 μm supported on carbon cloth have been successfully prepared. The entire surface of the H-TiO_2 NWs is covered uniformly by amorphous MnO_x with an average thickness of 7.0 nm. The H-TiO_2 NWs are poorly active for OER and the MnO_x as a major potential feasible electrocatalyst shows a considerable activity. The onset potential shifts negatively and current density improves not only by the surface area of MnO_x support on the H-TiO_2 NWs, but also by a synergistic effect between TiO_2 and MnO_x. The percentage of Mn^{2+} increases and the percentage of Mn^{3+} and Mn^{4+} decreases after 30 min chronopotentiometry test at 0.7 V in 0.1 mol L^{-1} solution, which prove the assume that the Mn^{4+} is firstly reduced to Mn^{3+} by electron injection from H_2O, then Mn^{3+} is further reduced to Mn^{2+} when the O_2 evolution happens for the OER in the alkaline media at pH ≥ 9. The presence of multiple valence manganese oxides in the H-TiO_2/MnO_x NWs is apt to occur the OER due to the electron transfer. This work of developing complex nanostuctured electrodes provides new insights into using transition metal oxide and carbon materials as high performance electrocatalyst for OER in water electrolysis.

Acknowledgements

This work was financially supported by the Natural Science Foundation of Guangdong Province (2014A030313521, 2014A030313529), the Guangdong Natural Science Foundation for Distinguished Young Scholar (2014A030306048), the National Natural Science Foundations of China (21276054, U1401246, 21376056), the Yang-cheng Scholars Foundation of Guangzhou (12A002D), and the Research Fund Program of Guangzhou Key chemical engineering and technology.

Notes and references

1 A. Bertin and J. P. Frangi, *Energ. Convers. Manage.*, 2013, **75**, 593–602.
2 A. Khalilnejad and G. H. Riahy, *Energ. Convers. Manage.*, 2014, **80**, 398–406.
3 D. Ghribi, A. Khelifa, S. Diaf and M. Belhamel, *Int J. Hydrogen Energ.*, 2013, **38**, 8480–8490.
4 M. Carmo, D. L. Fritz, J. Mergel and D. Stolten, *Int. J. Hydrogen Energ.*, 2013, ***38***, 4901–4934.
5 M. Y. Wang, Z. Wang, X. Z. Gong and Z. C. Guo, *Renew. Sust. Energ. Rev.*, 2014, **29**, 573–588.
6 L. Tao, X. D. Duan, C. Wang, X. F.Duan and S. Y. Wang, *Chem. Commun.*, 2015, **51**, 7470–7473.
7 Y. Surendranath, M. W. Kanan and D. G. Nocera, *J. Am. Chem. Soc.*, 2010, **132**, 16501–16509.
8 D. K. Bediako, Y. Surendranath and D. G. Nocera, *J. Am. Chem. Soc.*, 2013, **135**, 3662–3674.
9 R. Eisenberg and H. B. Gray, *Inorg. Chem.*, 2008, **47**, 1697–1699.
10 Y. Gorlin and T. F. Jaramillo, *J. Am. Chem. Soc.*, 2010, **132**, 13612–13614.
11 W. Hu, Y. Q. Wang, X. H. Hu, Y. Q. Zhou and S. L. Chen, *J. Mater. Chem.*, 2012, **22**, 6010–6016.
12 T. Reier, M. Oezaslan and P. Strasser, *ACS Catal.*, 2012, **2**, 1765–1772.
13 E. A. Paoli, F. Masini, R. Frydendal, D. Deiana, C. Schlaup, M. Malizia, T. W. Hansen, S. Horch, I. E. L. Stephens and I. Chorkendorff, *Chem. Sci.*, 2015, **6**, 190–196.
14 H. N. Nong, L. Gan, E. Willinger, D. Teschner and P. Strasser, *Chem. Sci.*, 2014, **5**, 2955–2963.
15 A. Minguzzi, O. Lugaresi, E. Achilli, C. Locatelli, A. Vertova, P. Ghigna and S. Rondinini, *Chem. Sci.*, 2014, **5**, 3591–3597.
16 H. G. S. Casalongue, M. L. Ng, S. Kaya, D. Friebel, H. Ogasawara and A. Nilsson, *Angew. Chem. Int. Ed.*, 2014, **53**, 7169–7172.
17 J. Y. Xu, D. Aili, Q. F. Li, E. Christensen, J. O. Jensen, W. Zhang, M. K. Hansen, G. Y. Liu, X. D. Wang and N. J. Bjerrum, *Energy Environ. Sci.*, 2014, **7**, 820–830.
18 S. K. Singh, V. M. Dhavale and S. Kurungot, *ACS Appl. Mater. Interfaces*, 2015, **7**, 442–451.
19 G. S. Hutchings, Y. Zhang, J. Li, B. T. Yonemoto, X. G. Zhou, K. K. Zhu and F. Jiao, *J. Am. Chem. Soc.*, 2015, **137**, 4223–4229.
20 M. E. G. Lyons and M. P. Brandon, *J. Electroanal. Chem.*, 2010, **641**, 119–130.
21 M. Fayette, A. Nelson and R. D. Robinson, *J. Mater. Chem. A*, 2015, **3**, 4274–4283.
22 P. W. Menezes, A. Indra, N. R. Sahraie, A. Bergmann, P. Strasser and M. Driess, *ChemSusChem*, 2015, **8**, 164–171.
23 F. Song and X. L. Hu, *J. Am. Chem. Soc.* 2014, **136**, 16481–16484.
24 A. Indra, P. W. Menezes, N. R. Sahraie, A. Bergmann, C. Das, M. Tallarida, D. Schmeißer, P. Strasser and M. Driess, *J. Am. Chem. Soc.*, 2014, **136**, 17530–17536.
25 L. Trotochaud, S. L. Young, J. K. Ranney and S. W. Boettcher, *J. Am. Chem. Soc.*, 2014, **136**, 6744–6753.
26 D. Tang, J. Liu, X. Y. Wu, R. H. Liu, X. Han, Y. Z. Han, H. Huang, Y. Liu and Z. H. Kang, *ACS Appl. Mater. Interfaces*, 2014, **6**, 7918–7925.
27 F. Rong, J. Zhao, P. P. Su, Y. Yao, M. R. Li, Q. H. Yang and C. Li, *J. Mater. Chem. A*, 2015, **3**, 4010–4017.
28 Y. F. Zhao, B. Sun, X. D. Huang, H. Liu, D. W. Su, K. N. Sun and G. X. Wang, *J. Mater. Chem. A*, 2015, **3**, 5402–5408.
29 C. Qiao, Y. Zhang, Y. Q. Zhu, C. B. Cao, X. H. Bao and J. Q. Xu, *J. Mater. Chem. A*, 2015, **3**, 6878–6883.
30 X. X. Zou, J. Su, R. Silva, A. Goswami, B. R. Sathe and T. Asefa, *Chem. Commun.*, 2013, **49**, 7522–7524.

31 L. Wang, C. Lin, D. K. Huang, F. X. Zhang, M. K. Wang and J. Jin, *ACS Appl. Mater. Interfaces*, 2014, **6**, 10172−10180.
32 Z. B. Zhuang, W. C. Sheng and Y. S. Yan, *Adv. Mater.*, 2014, **26**, 3950–3955.
33 Z. B. Zhuang, W. C. Sheng and Y. S. Yan, *ChemSusChem*, 2015, **8**, 659–664.
34 T. Takashima, K. Hashimoto and R. Nakamura, *J. Am. Chem. Soc.*, 2012, **134**, 18153–18156.
35 D. M. Robinson, Y. B. Go, M. Greenblatt and G. C. Dismukes, *J. Am. Chem. Soc.*, 2010, **132**, 11467–11469.
36 S. Chen, J. J. Duan, W. Han and S. Z. Qiao, *Chem. Commun.*, 2014, **50**, 207–209.
37 K. L. Pickrahn, S. WPark, Y. Gorlin, H. B. R. Lee, T. F. Jaramillo and S. F. Bent, *Adv. Energy Mater.*, 2012, **2**, 1269–1277.
38 M. S. El-Deab, M. I. Awad, A. M. Mohammad and T. Ohsaka, *Electrochem. Commun.*, 2007, **9**, 2082–2087.
39 A. Bergmann, I. Zaharieva, H. Dau and P. Strasser, *Energ. Environ. Sci.*, 2013, **6**, 2745–2755.
40 M. Huynh, D. K. Bediako and D. G. Nocera, *J. Am. Chem. Soc.*, 2014, **136**, 6002−6010.
41 R. Frydendal, E. Paoli, B. P. Knudsen, B. Wickman, P. Malacrida, I. E. L. Stephens and I. Chorkendorff, *ChemElectroChem*, 2014, **1**, 2075–2081.
42 Z. Y. Li, Z. L. Liu, J. C. Liang, C. W. Xu and X. H. Lu, *J. Mater. Chem. A*, 2014, **2**, 18236–18240.
43 Z. Y. Li, S. T. Shi, Q. S. Zhong, C. J. Zhang and C. W. Xu, *Electrochim. Acta*, 2014, **147**, 119–124.
44 R. Frydendal, M. Busch, N. B. Halck, E. A. Paoli, P. Krtil, I. Chorkendorff and J. Rossmeisl, *ChemCatChem*, 2015, **7**, 149–154.
45 C. H. Kuo, W. K. Li, L. Pahalagedara, A. M. El-Sawy, D. Kriz, N. Genz, C. Guild, T. Ressler, S. L. Suib and J. He, *Angew. Chem. Int. Ed.*, 2015, **54**, 2345 –2350.
46 M. R. Gao, Y. F. Xu, J. Jiang, Y. R. Zheng and S. H. Yu, *J. Am. Chem. Soc.*, 2012, **134**, 2930–2933.
47 W. Hu, S. Chen and Q. Xia, *Int. J. Hydrogen Energ.*, 2014, **39**, 6967–6976.
48 J. H. Lee and A. Selloni, *Phys. Rev. Lett.*, 2014, **112**, 196102.
49 L. L. Cai, I. S. Cho, M. Logar, A. Mehta, J. J. He, C. H. Lee, P. M. Rao, Y. Z. Feng, J. Wilcox, F. B. Prinz and X. L. Zhen, *Phys. Chem. Chem. Phys.*, 2014, **16**, 12299–12306.
50 M. J. Bierman and S. Jin, *Energ. Environ. Sci.*, 2009, **2**, 1050–1059.
51 S. J. Guo, S. Zhang, D. Su and S. H. Sun, *J. Am. Chem. Soc.*, 2013, **135**, 13879–13884.
52 C. Koenigsmann and S. S. Wong, *ACS Catal.*, 2013, **3**, 2031–2040.
53 J. L. Shui, C. Chen and J. C. M. Li, *Adv. Funct. Mater.*, 2011, **21**, 3357–3362.
54 Q. Liu, A. M. Asiri and X. P. Sun, *Electrochem. Commun.*, 2014, **49**, 21–24.
55 C. Jin, F. L. Lu, X. C. Cao, Z. R. Yang and R. Z. Yang, *J. Mater. Chem. A*, 2013, **1**, 12170–12177.
56 X. H. Lu, M. Yu, G. Wang, T. Zhai, S. Xie, Y. Ling, Y. X. Tong and Y. Li, *Adv. Mater.*, 2013, **25**, 267–272.
57 W. W. Xu, Z. Y. Lu, X. D. Lei, Y. P. Li and X. M. Sun, *Phys. Chem. Chem. Phys.*, 2014, **16**, 20402–20405.
58 C. B. Ouyang, X. Wang, C. Wang, X. X.Zhang, J. H. Wu, Z. L. Ma, S. Dou and S. Y.Wang, *Electrochim. Acta*, 2015, **174**, 297–301.
59 P. Chetri, P. Basyach and A. Choudhury, *J. Solid. State. Chem.*, 2014, **220**, 124–131.
60 X. N. Lu, C. Y. Song, C. C. Chang, Y. X. Teng, Z. S. Tong and X. L. Tang, *Ind. Eng. Chem. Res.*, 2014, **53**, 11601−11610.
61 J. W. Li, P. Zhao and S. T. Liu, *Appl. Catal. A–Gen.*, 2014, **482**, 363–369.
62 A. Ramírez, P. Hillebrand, D. Stellmach, M. M. May, P. Bogdanoff and S. Fiechter, *J. Phys. Chem. C*, 2014, **118**, 14073−14081.
63 M. X. Wang, P. Y. Zhang, J. G. Li and C. J. Jiang, *Chinese J. Catal.*, 2014, **35**, 335–341.
64 Y. Gorlin, C. J. Chung, J. D. Benck, D. Nordlund, L. Seitz, T. C. Weng, D. Sokaras, B. M. Clemens and T. F. Jaramillo, *J. Am. Chem. Soc.*, 2014, **136**, 4920–4926.
65 F. X. Yin, G. R. Li and H. Wang, *Catal. Commun.*, 2014, **54**, 17–21.
66 C. C. McCrory, S. Jung, J. C. Peters and T. F. Jaramillo, *J. Am.Chem. Soc.*, 2013, **135**, 16977–16987.
67 Y. T. Meng, W. Q. Song, H. Huang, Z. Ren, S. Y. Chen and S. L. Suib, *J. Am. Chem. Soc.*, 2014, **136**, 11452–11464.
68 X. Long, J. K. Li, S. Xiao, K. Y. Yan, Z. L. Wang, H. N. Chen and S. H. Yang, *Angew. Chem. Int. Ed.*, 2014, **53**, 7584–7588.
69 T. Takashima, K. Hashimoto and R. Nakamura, *J. Am. Chem. Soc.*, 2012, **134**, 1519–1527.

A table of contents

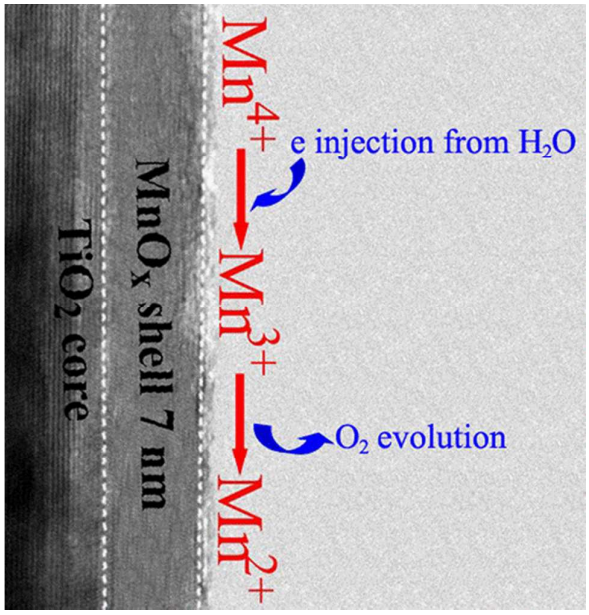

Manganese oxides/hydrogenated TiO_2 core-shell nanowires exhibited enhanced electrocatalytic activity toward oxygen evolution reaction in water electrolysis